In situ synthesis of magnetic iron oxide nanoparticles in chitosan hydrogels as a reaction field: Effect of cross-linking density

doi: https://doi.org/10.1016/j.colsurfb.2019.04.004

Graphical Abstract

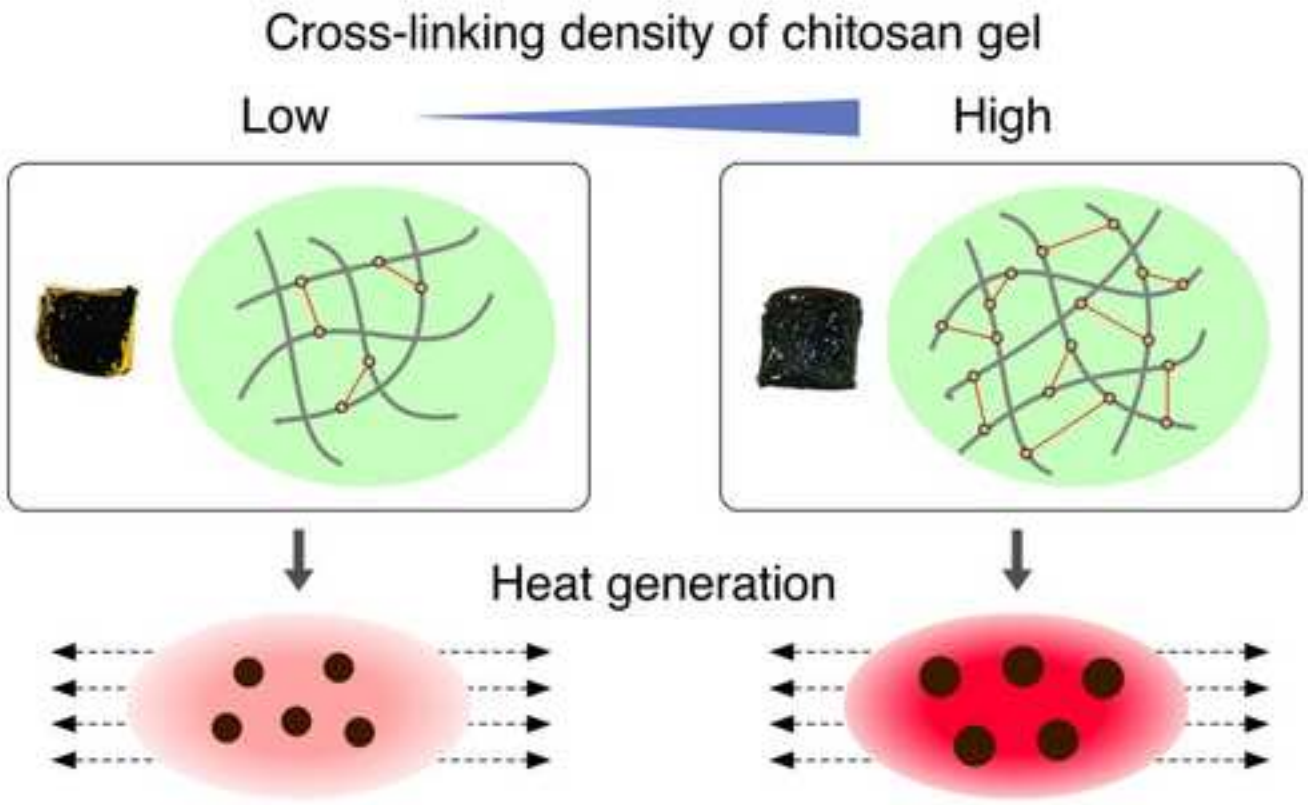

Graphical abstract

In situ Synthesis of Magnetic Iron Oxide Nanoparticles in Chitosan Hydrogels as a Reaction Field: Effect of Cross-linking Density

Toshiki Miyazaki[1], Akiko Iwanaga[1], Yuki Shirosaki[2] and Masakazu Kawashita[3]

[1]Graduate School of Life Science and Systems Engineering, Kyushu Institute of Technology, Kitakyushu, Japan

[2]Faculty of Engineering, Kyushu Institute of Technology, Kitakyushu, Japan

[3]Graduate School of Biomedical Engineering, Tohoku University, Sendai, Japan

Corresponding author: Toshiki Miyazaki

Graduate School of Life Science and Systems Engineering, Kyushu Institute of Technology, 2-4, Hibikino, Wakamatsu-ku, Kitakyushu 808-0196, Japan

Tel/Fax: +81-93-695-6025

E-mail: tmiya@life.kyutech.ac.jp

Short statistical summary: 3,253 words, 0 tables and 8 figures

Abstract

Magnetic iron oxides such as magnetite and γ-hematite have attracted considerable attention as thermoseeds for hyperthermia treatment because of their ability to generate heat under an alternating magnetic field. Control of the particle size and their combination with biocompatible polymers are expected to be beneficial for optimization of the nanoparticles. These processes can be accomplished through the synthesis of magnetite in gels, as the network structure of the polymer gel can control the grain growth of the magnetite. However, the effect of the cross-linking density of the gels remains unclear. In this study, we synthesized magnetic iron oxides *in situ* in chitosan hydrogels with different cross-linking densities and examined the crystalline structure and heat generation under alternating magnetic field. The crystalline phase and amount of magnetite were observed to be dependent on the cross-linking density of the gel, and the heat generation of the nanoparticles was governed by their crystalline structure and particle size rather than solely the amount of formed iron oxide.

Keywords

Iron oxide nanoparticle, Chitosan, Cross-linking density, Hyperthermia, Heat generation

1. Introduction

Nanoparticles of magnetic iron oxide such as magnetite (Fe_3O_4) and γ-hematite (γ-Fe_2O_3) can be used for medical applications such as MRI contrast agents [1,2]. Furthermore, because of their ability to generate heat under an alternating magnetic field, magnetic iron oxide nanoparticles have attracted attention as a material for cancer hyperthermia treatment [3-5]. The hybridization of magnetic iron oxides and organic substances for control of the crystalline phase, biological affinity, and drug-release properties has attracted considerable attention [6-9]. Furthermore, synthesis of the magnetic iron oxide in the gel would enable the above functionalization to be achieved *in situ*, simplifying the production process.

Several attempts have been made to diffuse iron ions into a polymer gel from outside the gel followed by precipitation of the iron oxide inside the gel by subsequent alkali treatment. Liu *et al.* prepared an iron oxide in agarose gel combined with nanocellulose and polypyrrole to provide electron conductivity [10]. Wang *et al.* demonstrated the formation of superparamagnetic Fe_3O_4 in chitosan gel and observed that its content increased with decreasing pH [11]. Zhang *et al.* showed that iron oxide was formed in

chitosan gel under magnetic-field irradiation and that the crystallinity and orientation increased with increasing magnetic field strength [12]. In addition, *in situ* precipitation of Fe_3O_4 in polymer blend of silk fibroin and hydroxypropyl methyl cellulose has been attempted [13]. Composite microspheres of Fe_3O_4 and chitosan can be also fabricated by using a syringe-assisted pump device [14]. The network structure of the gel also governs ion diffusion and the crystalline structure of the resultant precipitates as the state of the intermolecular reaction field can be changed. Heat generation ability is drastically changed by particle size of the magnetic nanoparticles for hyperthermia applications [4]. In addition, injectable hybrid of Fe_3O_4 and polymer hydrogel with low cross-linking density is expected to show embolization effect as well as hyperthermia [15]. However, details on the effects of the gel structure on the crystalline structure, particle size, and heat generation in the alternating magnetic field of iron oxides require further investigation.

In the present study, iron oxide formation was attempted in chitosan gels with different cross-linking densities, and the effects of the density on the nanostructure and heat-generation ability were investigated. Fe_3O_4 nanoparticles have been popularly prepared by coprecipitation of both Fe^{2+} and Fe^{3+} in alkaline solution. In the present study,

according to the report that they can be also obtained by precipitation of Fe^{2+} and subsequent oxidation by air at above 50°C [16], only $FeCl_2$ was used for a source of iron.

2. Materials and methods

2.1 Synthesis of gel precipitated with iron oxide

First, 2.0 g of chitosan (Grade F, 80%–90% degree of deacetylation, Kimica Co., Tokyo, Japan) was added to 100 mL of 0.05 M acetic acid (Wako Pure Chemical Industries, Ltd. Osaka, Japan) aqueous solution with stirring. Then, glutaraldehyde (GLA; 24.0%–26.0% purity, Wako Pure Chemical Industries, Ltd.) solution was added to the solution as a cross-linking agent with molar ratios ranging from 0.5 to 3.0 with respect to the amino group of the chitosan. The samples with molar ratios of 0.5, 1.0, 2.0, and 3.0 are hereafter denoted as ChG05, ChG10, ChG20, and ChG30, respectively. Next, the mixed solution was stirred for 5 min and then allowed to stand at room temperature. The obtained gels were cut to volumes of 1.2 cm^3, and Fe^{2+} was incorporated into the gels by immersing in 40 mL of an aqueous solution of 0.1 M iron chloride (II) ($FeCl_2$, Wako Pure Chemical Industries, Ltd.) solution for 6 h at room temperature. After washing with

ultrapure water, the gels were immersed in 0.5 M NaOH (Kanto Chemical Co., Inc., Tokyo, Japan) aqueous solution at 60°C for various periods within 12 h using a water bath (Personal H-10, Taitec Co., Nagoya, Japan). The treated gels were washed with ultrapure water until a neutral surface pH was achieved. Finally, the gels were freeze-dried at −80°C using a freeze drier (FRD-830M, Asahi Techno Glass Co., Ltd., Shizuoka, Japan).

2.2 Sample characterization

The cross-linking density of each gel was determined by measuring the amount of free amino groups present in the gel using a ninhydrin coloring solution kit (Wako Pure Chemical Industries, Ltd.) [17,18]. Namely, the absorption of Ruhemann's purple at 570 nm generated by the reaction of ninhydrin and the amino group was measured using UV–vis spectrophotometry (V-630, JASCO Co., Tokyo, Japan). The cross-linking density was calculated as ratio of the free amino groups in the gel to that of the original chitosan.

The ratio of the weight change of the gels (R) after immersion in the iron chloride solution was calculated using equation (1):

$$R= \frac{100(Wa-W_b)}{W_b}, \qquad (1)$$

where W_b and W_a are the weight of the gel before and after immersion, respectively.

The crystalline structure of each gel was analyzed using X-ray diffraction (XRD; MXP3V, Mac Science Co., Ltd., Yokohama, Japan). CuKα radiation was used as the X-ray source, and the voltage and current of the Cu tube were 40 kV and 30 mA, respectively. The incident angle of the X-ray was fixed at 1°, and the step width and counting time were 0.020° and 4 s, respectively.

The thermal properties were analyzed using thermogravimetry/differential thermal analysis (TG-DTA; TGDTA2000S, Mac Science, Co., Ltd.). For TG-DTA, the temperature was increased from room temperature to 600°C at a rate of 10°C/min and held for 30 min. Measurements of pure chitosan were also performed for comparison.

The morphology of the iron oxide nanoparticles was analyzed using transmission electron microscopy (TEM; JEM-3010, JEOL Ltd., Tokyo, Japan) with an acceleration voltage of 200 kV. For the TEM observation, the chitosan matrix in the samples was

decomposed in advance. Namely, 5 mg of the powder sample was added to a solution prepared from 10 mg of Yatalase (chitosanase activity: 19 $U \cdot g^{-1}$, Takara Bio Inc., Shiga Japan) and 30 mL of 0.1 M phosphate buffer solution (pH 7.2), and the mixture was stored at 37.5°C for 1 day. After decomposition of chitosan, the nanoparticles were collected by centrifugation (CN-2060, As One Co., Tokyo, Japan) at 6000 rpm for 20 min.

2.3 Heat generation measurement

To determine the heat generation of the sample, the temperature increase in an alternating magnetic field was measured, and the specific absorption rate (SAR) was calculated from the temperature [19]. The gels (0.25 g) treated with 0.5 M NaOH aqueous solution were immersed in 1 mL of 1.0 mass% boiling aqueous solution of agar (Wako Pure Chemical Industries, Ltd.) and then cooled to room temperature. A glass bottle containing the gel was placed in an alternating magnetic field with a frequency of 100 kHz and magnetic field strength of 300 Oe. The temperature change of the sample was measured using a fiber optic thermometer (OTG-MPK5, Opsens Inc., Quebec,

Canada) attached to a signal conditioner (TempSens, Opsens Inc., Quebec, Canada). The SAR value was calculated using equation (2):

$$SAR = \frac{\sum_i c_i m_i}{m_{Fe}} \frac{\Delta T}{\Delta t}, \qquad (2)$$

where c_i and m_i are the heat capacity (C_{agar} = 4.18 J/g·K, C_{Fe3O4} = 0.67 J/g·K, $C_{chitosan}$ = 0.11 J/g·K) and mass of each component, respectively, and ΔT/dt is the initial gradient of the time-dependent temperature curve (Δt = 60 s).

3. Results

The cross-linking density increased in the order of ChG05 (10.2±2.2%) < ChG10 (31.9±3.1%) < ChG20 (89.8±1.4%) < ChG30 (96.2±0.8%) (n=3). Figure 1 shows the ratio of the weight change of the gels with different cross-linking densities after immersion in $FeCl_2$ solution. The weight decreased with increasing immersion time for all the samples. Moreover, the degree of the weight loss increased with increasing cross-linking density. As observed in Fig. 2, the amount of the inorganic component slightly decreased with increasing cross-linking density.

XRD patterns of the samples are presented in Fig. 3. γ-Fe_2O_3, Fe_3O_4, and δ-FeOOH were detected for all the samples. In addition, α-FeOOH was detected for ChG05 and ChG10. The peak intensities of magnetic γ-Fe_2O_3 and Fe_3O_4 increased with increasing cross-linking density. It is generally considered difficult to distinguish Fe_3O_4 and γ-Fe_2O_3 using XRD because they have the same spinel structure and almost identical lattice parameters. However, identification of their mixture using step-scanned XRD can be performed because of the slight difference in their peak positions [20]. As the diffraction peaks at approximately 35.5° in 2θ are asymmetrical and a shoulder can be observed at higher diffraction angle, both Fe_3O_4 and γ-Fe_2O_3 were considered to form for all the samples.

Figure 4 presents TEM images of the samples. Spherical particles ranging in size from 3 to 10 nm were observed for all the samples. Rod-like particles with lengths of approximately 10 nm were also observed for ChG05.

Figure 5 shows the particle size distribution and the number of rod-like particles calculated from the TEM images. The average particle size was approximately 5 nm for

ChG05, ChG10, and ChG20 but increased to 13 nm for ChG30. In addition, more rod-like particles were observed for the samples with lower cross-linking density.

Figure 6 presents XRD patterns of ChG05 and ChG30 immersed in 0.5 M NaOH solution for various periods within 12 h. For ChG5, the peaks of γ-Fe_2O_3 and Fe_3O_4 were broad and low within 3 h and became sharp with slightly increased intensities after 12 h. However, for ChG30, the peaks were sharper and their intensities were higher than those for ChG05. After 12 h, the peaks of α-FeOOH remained for ChG05, whereas they disappeared for ChG30. The relative intensity of the δ-FeOOH peak to those of γ-Fe_2O_3 and Fe_3O_4 was also higher for ChG5 than for ChG30.

Figure 7 shows the change in temperature of the samples embedded in agar gels in the alternating magnetic field. Directly before applying the magnetic field, the temperature was 25°C–30°C. The degree of the temperature increase for ChG05 and ChG10 after 10 min was approximately 3°C, whereas that for ChG20 and ChG30 was 15°C or more. Vigorous heat generation was observed for the samples with higher cross-linking density. The calculated SAR value increased in the order of ChG05 (13.7 $W \cdot g^{-1}$) < ChG10 (24.0 $W \cdot g^{-1}$) < ChG20 (96.5 $W \cdot g^{-1}$) < ChG30 (112.2 $W \cdot g^{-1}$), indicating

that the heat generation efficiency of the samples per mass improved with increasing cross-linking density.

4. Discussion

Our findings indicate that iron oxide nanoparticles can be synthesized *in situ* using chitosan gel with controlled cross-linking density as a reaction field. The weight of the gel decreased after soaking in $FeCl_2$ solution irrespective of cross-linking density (see Fig. 1). Weight of water diffusing from the gel into surrounding fluid by difference in osmotic pressure would be higher than that of incorporated Fe^{2+}. The amount of iron oxide produced in the chitosan gel decreased with increasing cross-linking density (see Fig. 2). In addition, the weight loss of the gel increased with increasing cross-linking density (see Fig. 1). Therefore, iron oxide formation is considered to be suppressed because the chitosan gel with high cross-linking density was slightly swelled and the uptake of Fe^{2+} was suppressed.

Iron oxide nanoparticles with larger crystallite size were produced in the chitosan gel with increasing cross-linking density, although the content of the total inorganic

component decreased (see Figs. 4 and 5). Figure 8 presents a schematic illustration of the nucleation and particle growth of Fe_3O_4 inside a gel for different cross-linking densities. With increasing cross-linking density, the amount of uncross-linked amino groups in the gel able to adsorb Fe^{2+} decreased. Therefore, the number of nucleation sites of Fe_3O_4 decreased.

Focusing on the initial process of the iron oxide formation, the rapid formation of δ-FeOOH in ChG30 within 5 min is considered to contribute to the formation of a large amount of Fe_3O_4. Enomoto *et al.* analyzed the precipitate formed by the reaction of Fe^{2+} salt with NaOH solution under ultrasonic irradiation using XRD [21]. The crystalline phase of the precipitate was $Fe(OH)_2$ in the wet state immediately after the reaction but completely transformed to δ-FeOOH after drying via the following reaction:

$$4Fe(OH)_2 + O_2 \rightarrow 4\delta - FeOOH + 2H_2O \qquad (3)$$

The same phenomenon occurred in this study, as the sample was freeze-dried before the XRD measurement. Therefore, the rapid formation of $Fe(OH)_2$ as an intermediate of Fe_3O_4 would result in a large amount of Fe_3O_4 in ChG30.

Not only Fe_3O_4 but also γ-Fe_2O_3 was formed in the chitosan gels. γ-Fe_2O_3 has been reported to be formed by the dehydration of α- or γ-FeOOH [22,23] or air oxidation of Fe_3O_4 [24,25]. It has been reported that the crystalline phase of FeOOH synthesized from iron chloride as a starting material is not γ-FeOOH but α-FeOOH or β-FeOOH [26]. Therefore, the present γ-Fe_2O_3 formation is considered to mainly result from the dehydration of α-FeOOH or oxidation of Fe_3O_4.

In the chitosan gels with low cross-linking density, the formation of non-magnetic FeOOH was promoted (see Figs. 3 and 4). Dissolved oxygen tends to diffuse at low cross-linking density, resulting in oxidation of Fe^{2+} to give FeOOH. Furthermore, it has been reported that Fe^{3+} adsorbs on the amino and hydroxyl groups of chitosan under the alkaline condition of pH 12 [27]. Therefore, it is assumed that Fe^{2+} is adsorbed on such functional groups, with a high amount remaining in the chitosan gel with low cross-linking density, and is easily oxidized by the dissolved air.

Overall reactions in the present composite can be summarized as follows:

(Fe_3O_4 formation)

$$Fe^{2+} + 2OH^- \rightarrow Fe(OH)_2 \qquad (4)$$

$$6Fe(OH)_2 + O_2 \rightarrow 2Fe_3O_4 + 6H_2O \qquad (5)$$

(FeOOH formation)

$$4Fe(OH)_2 + O_2 \rightarrow 4\alpha, \delta - FeOOH + 2H_2O \qquad (6)$$

(γ-Fe_2O_3 formation)

$$2FeOOH \rightarrow \gamma - Fe_2O_3 + H_2O \qquad (7)$$

$$4Fe_3O_4 + O_2 \rightarrow 6\gamma - Fe_2O_3 \qquad (8)$$

ChG30 exhibited excellent heat-generation characteristics despite the small amount of inorganic component in the chitosan gel (see Figs. 2 and 7). Jeyadevan *et al.* reported the theoretical heat generation of Fe_3O_4 nanoparticles via Néel and Brownian relaxation at a frequency of 600 kHz and magnetic field intensity of 40 Oe [4]. The total heat generation reached a maximum at a particle size of approximately 12 nm, and almost no dissipation was observed below 8 nm. Therefore, it is considered that a large amount of Fe_3O_4 particles with sizes of more than 10 nm would contribute to a high heat generation ability. This finding is consistent with the TEM images in Fig. 4.

Notably, ChG20 exhibited heat-generation ability comparable to that of ChG30 despite its similar average particle size to ChG5 and ChG10 (see Figs. 5 and 7). A small

amount of particles with sizes of 10–13 nm were observed in ChG20 but not in ChG5 or ChG10 (see Fig. 5). Furthermore, the amount of non-magnetic rod-like FeOOH particles in ChG20 was also smaller than that in ChG5 or ChG10 (see Fig. 5). These findings are considered to contribute to the high heat-generation ability of ChG20.

This study revealed that the cross-linking structure of the gel also governs the nanostructure of the precipitated inorganic phase through aqueous processing. It is known that the chemical state of inorganic ions as a precursor is also affected by the functional groups of the coexisting organic phase. In the future, it would be useful to investigate the effects of the functional groups of the gels to establish general principles for the organic–inorganic interaction during the synthesis of inorganic materials.

5. Conclusions

In this study, *in situ* synthesis of magnetic iron oxide nanoparticles in chitosan gels with different cross-linking densities was performed, and the relationship between the cross-linking density and crystalline structure of the nanoparticles and heat generation under alternating magnetic field was investigated. With increasing cross-linking density,

the amount of the formed inorganic phase decreased but the heat generation in the alternating magnetic field was enhanced, indicating that the heat-generation property was not governed solely by the total amount of iron oxide. Namely, even if the amount of the inorganic component was not large, a chitosan–iron oxide hybrid with excellent heat-generation ability can be produced with appropriate selection of the gel structure. Overall, our findings provide fundamental guidelines for the design of biocompatible organic–inorganic hybrids with heat-generation ability for hyperthermia treatment.

Disclosure

The authors report no conflicts of interest in this work.

Acknowledgments

The authors would like to thank Tiffany Jain, M.S., from Edanz Group (www.edanzediting.com/ac) for editing a draft of this manuscript.

References

1. M. Mitsumori, M. Hiraoka, T. Shibata, Y. Okuno, S. Masunaga, M. Koishi, K. Okajima, Y. Nagata, Y. Nishimura, M. Abe, K. Ohura, M. Hasegawa, H. Nagae, Y. Ebisawa, Int. J. Hyperthermia, 10 (1994) 785.
2. C. Pereira, A.M. Pereira, M. Rocha, C. Freire and C.F.G.C. Geraldes, J. Mater. Chem. B, 3 (2015) 6261.
3. Z. Li, M. Kawashita, N. Araki, M. Mitsumori, M. Hiraoka, M. Doi, Mater. Sci. Eng. C, 30 (2010) 990.
4. B. Jeyadevan, J. Ceram. Soc. Japan, 118 (2010) 391.
5. A. Sudame, G. Kandasamy, D. Maity, J. Nanosci. Nanotech., 19 (2019) 3991.
6. B. Wang, C. Xu, J. Xie, Z. Yang, S. Sun, J. Am. Chem. Soc., 130 (2008) 14436.
7. G. Li, Y. Jiang, K. Huang, P. Ding, J. Chen, J. Alloys Compd., 466 (2008) 451.
8. Y. Kuwahara, T. Miyazaki, Y. Shirosaki and M. Kawashita, RSC Adv., 4 (2014) 23359.
9. E.L. Brito, D.N. Gomes, C.C. Plá Cid, J.C.R. de Araújo, F. Bohn, L. Streck, J. L.C. Fonseca, Colloid Surface A, 560 (2019) 376.
10. K. Liu, L. Chen, L. Huang, Y. Ni, Z. Xu, S. Lin, H. Wang, Cellulose, 25 (2018)

4565.

11. Y. Wang, B. Li, Y. Zhou, D. Jia, Polym. Adv. Technol., 19 (2008) 1256.
12. W. Zhang, S. Jia, Q. Wu, S. Wu, J. Ran, Y. Liu, J. Hou, Mater. Sci. Eng. C, 32 (2012) 381.
13. K. Luo, Z. Shao, Chin. J. Polym. Sci., 35 (2017) 515.
14. M.E. Villamin, Y. Kitamoto, AIP Conf. Proc., 2067 (2019) 020016.
15. F. Zhou, L. Chen, Q. An, L. Chen, Y. Wen, F. Fang, W. Zhu, T. Yi, Sci. Rep., 6 (2016) 32145.
16. M. Kiyama, Bull. Chem. Soc. Japan, 47 (1974) 1646.
17. F. L. Mi, Y. C. Tan, H. C. Liang, R. N. Huang, H. W. Sung, J. Biomater. Sci. Polym. Ed., 12 (2001) 835.
18. Y. Shirosaki Y, K. Tsuru, S. Hayakawa, A. Osaka, M.A. Lopes, J.D. Santos, M.A. Costa, M.H. Fernandes, Acta. Biomater. 5 (2009) 346.
19. M. Kawashita, S. Domi, Y. Saito, M. Aoki, Y. Ebisawa, T. Kokubo, T. Saito, M. Takano, N. Araki, M. Hiraoka, J. Mater. Sci.: Mater. Med., 19 (2008) 1897.
20. W. Kim, C.Y. Suh, S.W. Cho, K.M. Roh, H. Kwon, K. Song, I.J. Shon, Talanta, 94

(2012) 348.

21. N. Enomoto, J. Akagi, Z. Nakagawa, Ultrason. Sonochem., 3 (1996) S97.

22. T.S. Gendler, V.P. Shcherbakov, M.J. Dekkers, A.K. Gapeev, S.K. Gribov, E. McClelland, Geophys. J. Int., 160 (2005) 815.

23. T. Ahn, J.H. Kim, H.-M. Yang, J. W. Lee, J.-D. Kim, J. Phys. Chem. C, 116 (2012) 6069.

24. J.-P. Jolivet, C. Chanéac, E. Tronc, Chem. Commun., 2004 (2004) 481.

25. J. A. Cuenca, K. Bugler, S. Taylor, D. Morgan, P. Williams, J. Bauer, A. Porch, J. Phys.: Condens. Matter, 28 (2016) 106002.

26. M. Kiyama, T. Takada, Bull. Chem. Soc. Japan, 45 (1972) 1923.

27. C. Shen, Y. Shen, Y. Wen, H. Wang, W. Liu, Water Res., 45 (2011) 5200.

Figure captions

Figure 1 Ratio of the weight change of the gels with different cross-linking densities after immersion in $FeCl_2$ solution (n=3).

Figure 2 Relationship between the cross-linking density and inorganic component in the gels (n=3).

Figure 3 XRD patterns of the samples after immersion in 0.5 M NaOH solution for 12 h.

Figure 4 TEM images of the samples after immersion in 0.5 M NaOH solution for 12 h.

Figure 5 Particle size distribution and the number of rod-like particles calculated from TEM images.

Figure 6 XRD patterns of ChG05 and ChG30 immersed in 0.5 M NaOH solution for various periods within 12 h.

Figure 7 Change in temperature of the samples embedded in agar gels in alternating magnetic field.

Figure 8 Schematic illustration of nucleation and particle growth of Fe_3O_4 inside gels with different cross-linking densities.

Figure(s)
Click here to download high resolution image

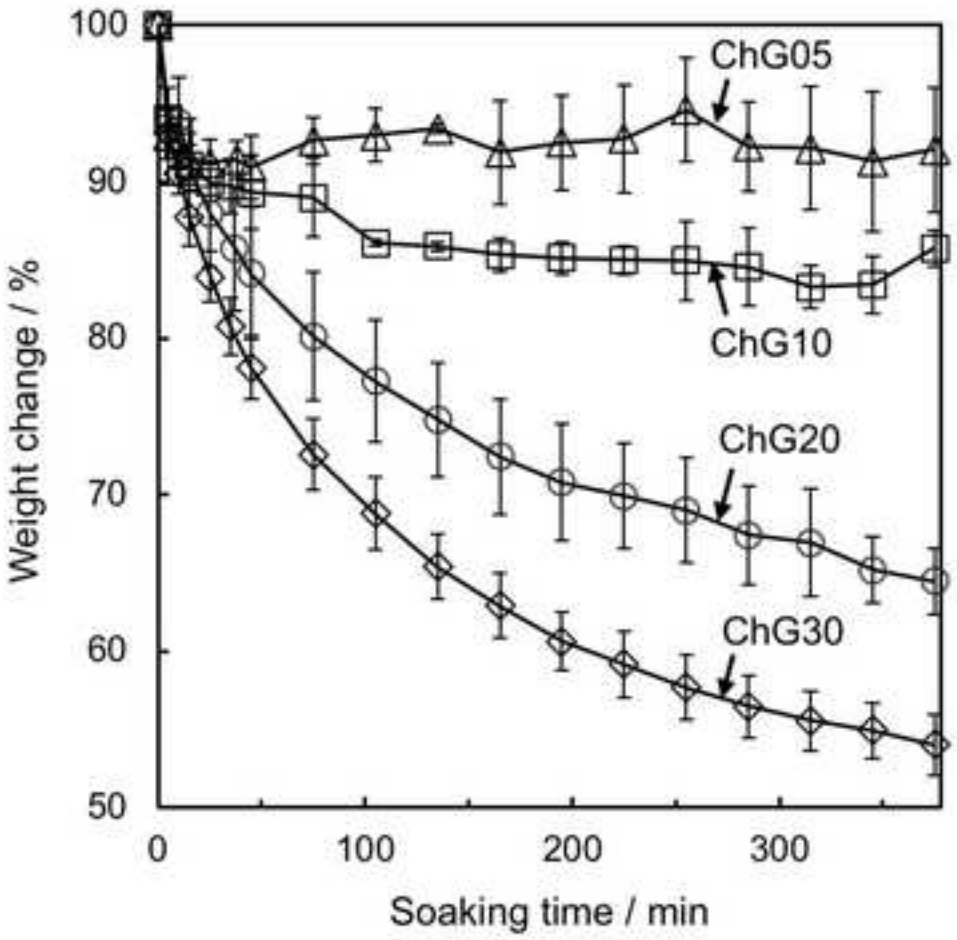

Figure 1

Figure(s)

Click here to download high resolution image

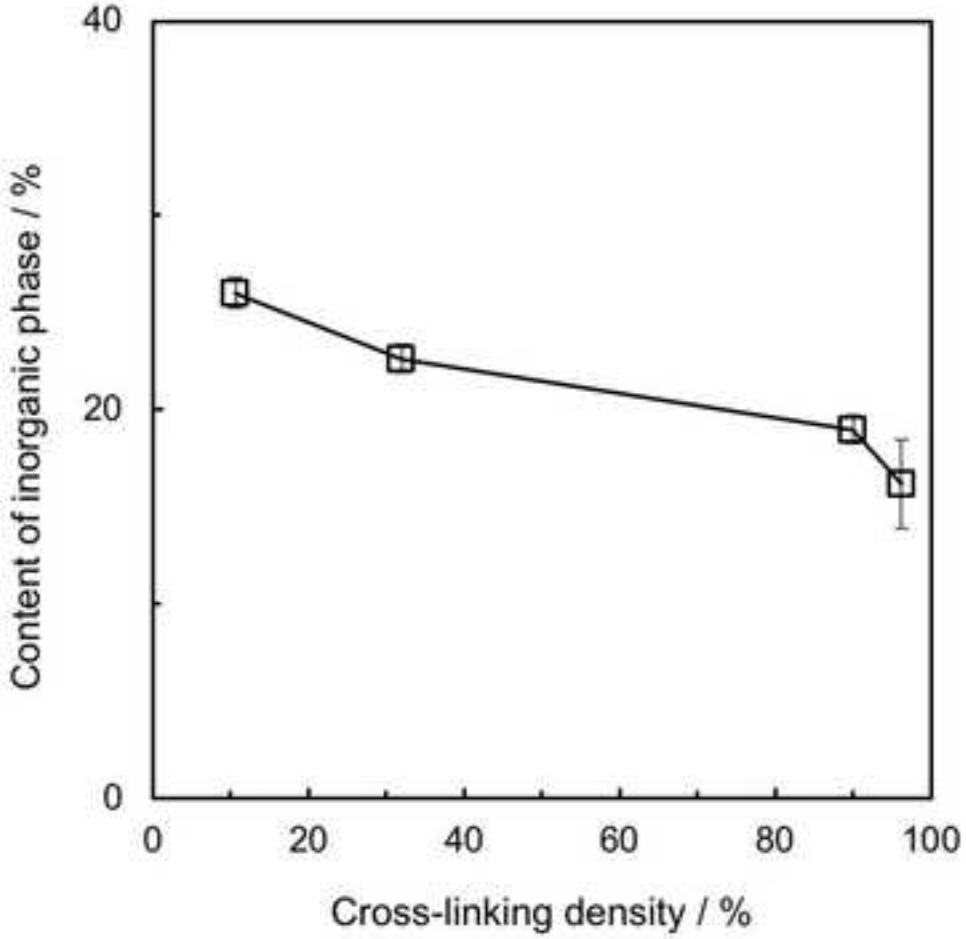

Figure 2

Figure(s)

Click here to download high resolution image

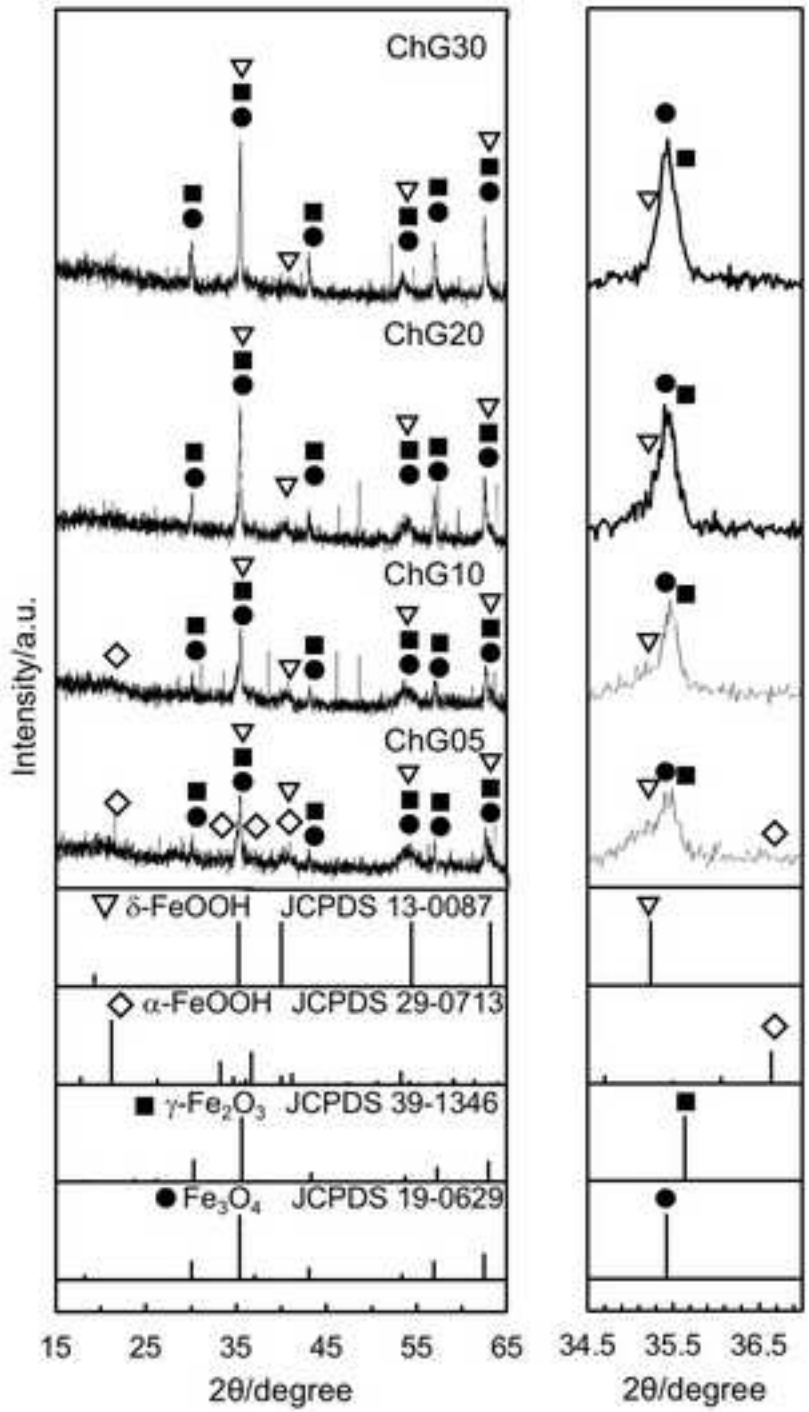

Figure 3

Figure(s)

Click here to download high resolution image

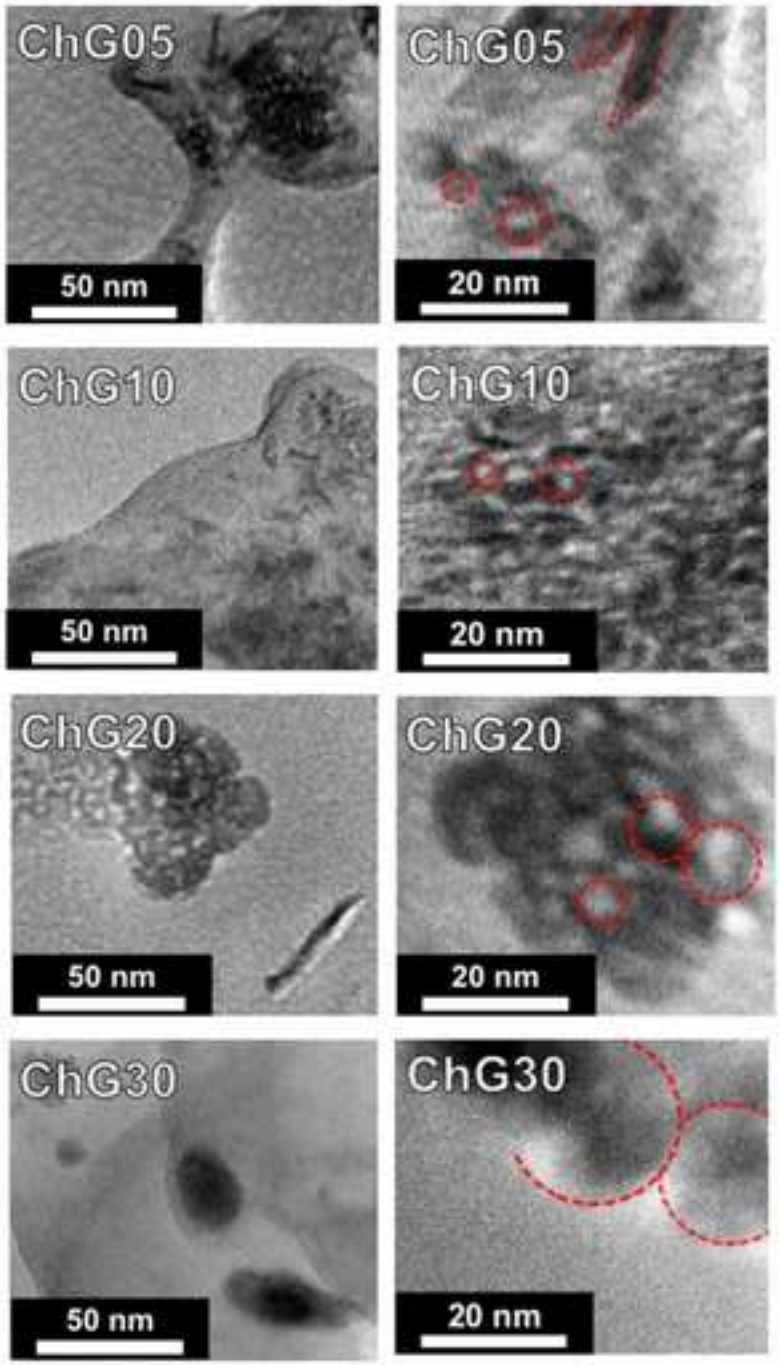

Figure 4

Figure(s)

Click here to download high resolution image

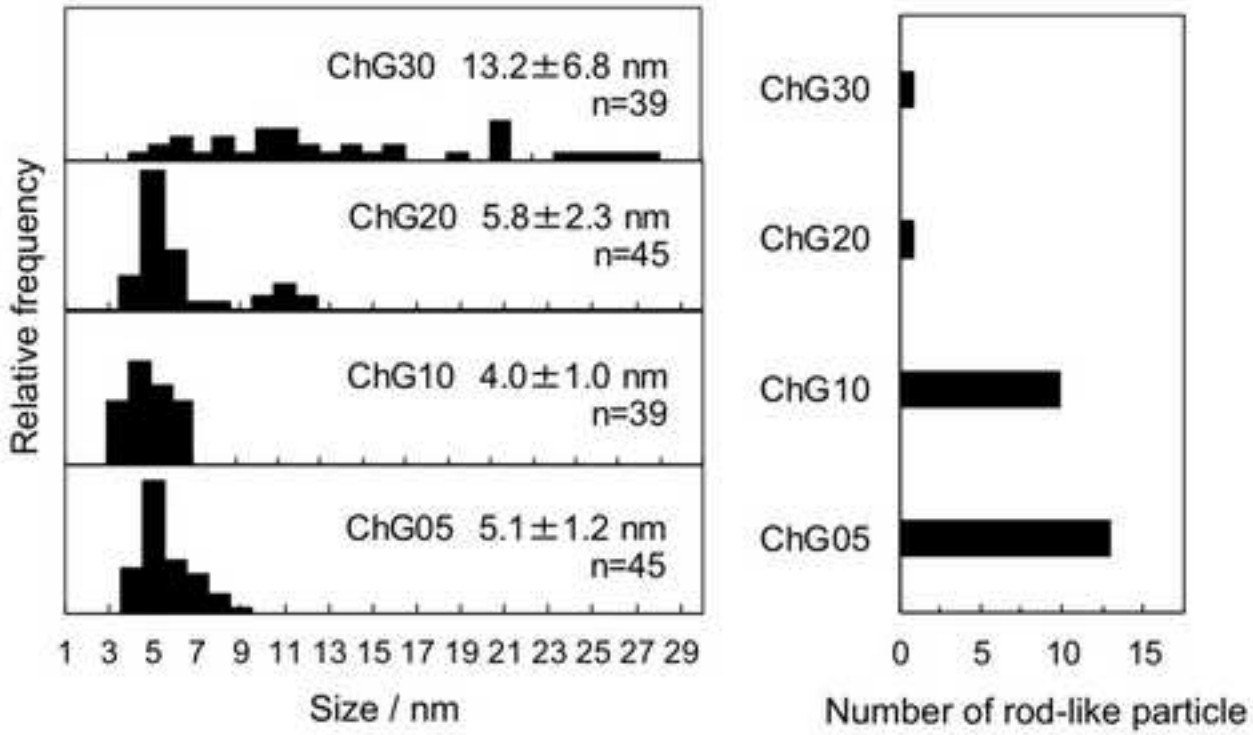

Figure 5

Figure(s)

Click here to download high resolution image

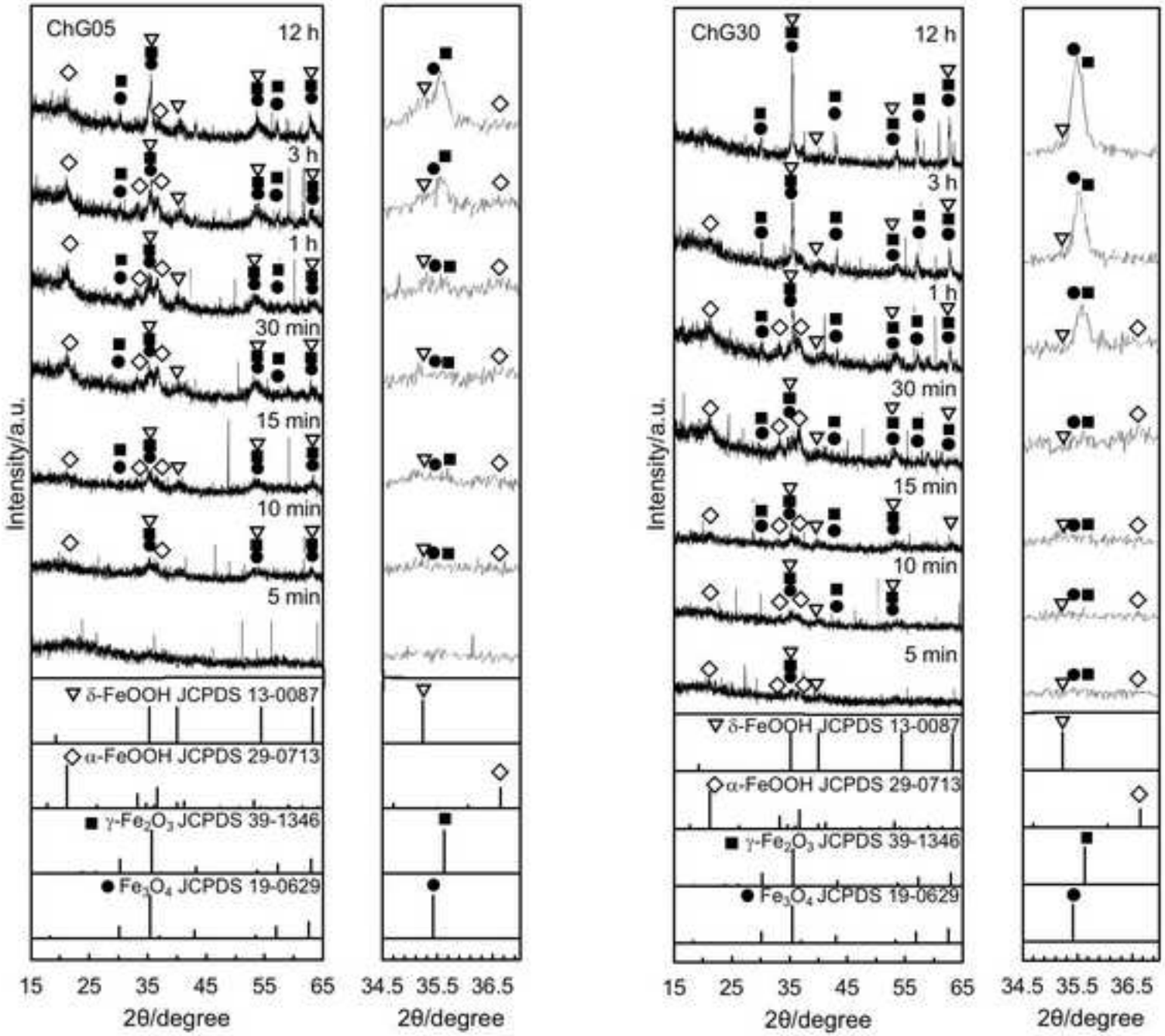

Figure 6

Figure(s)
Click here to download high resolution image

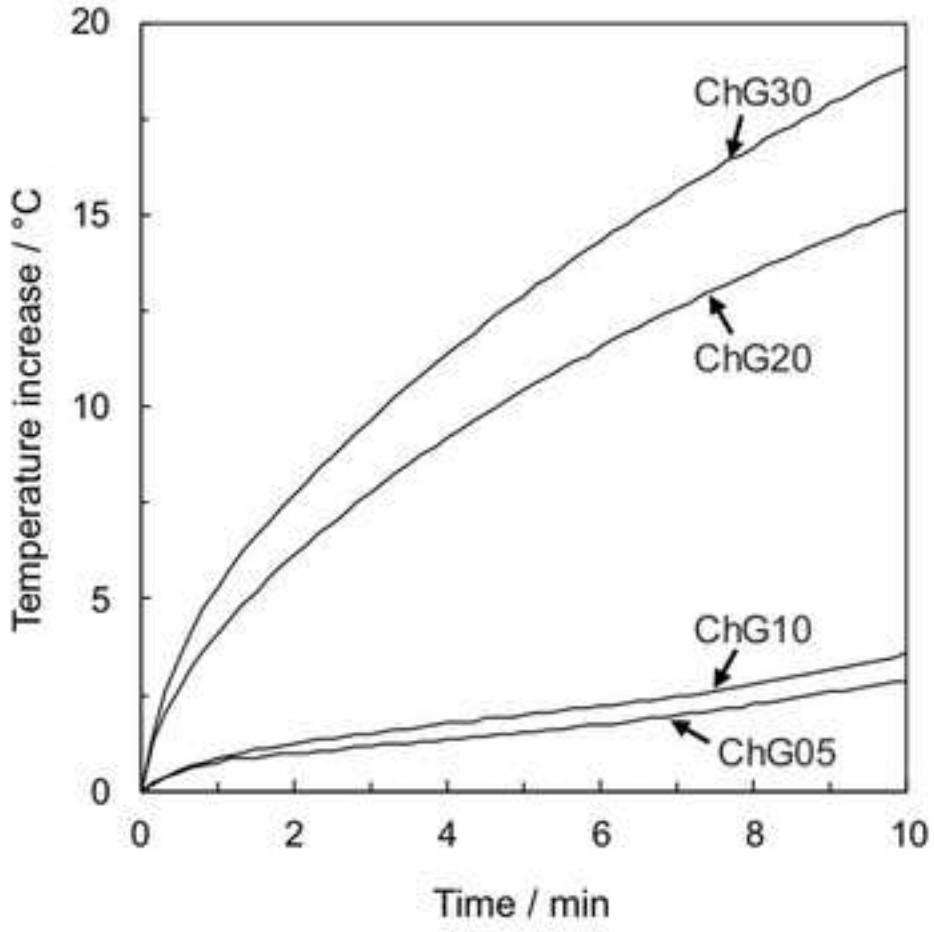

Figure 7

Figure(s)
Click here to download high resolution image

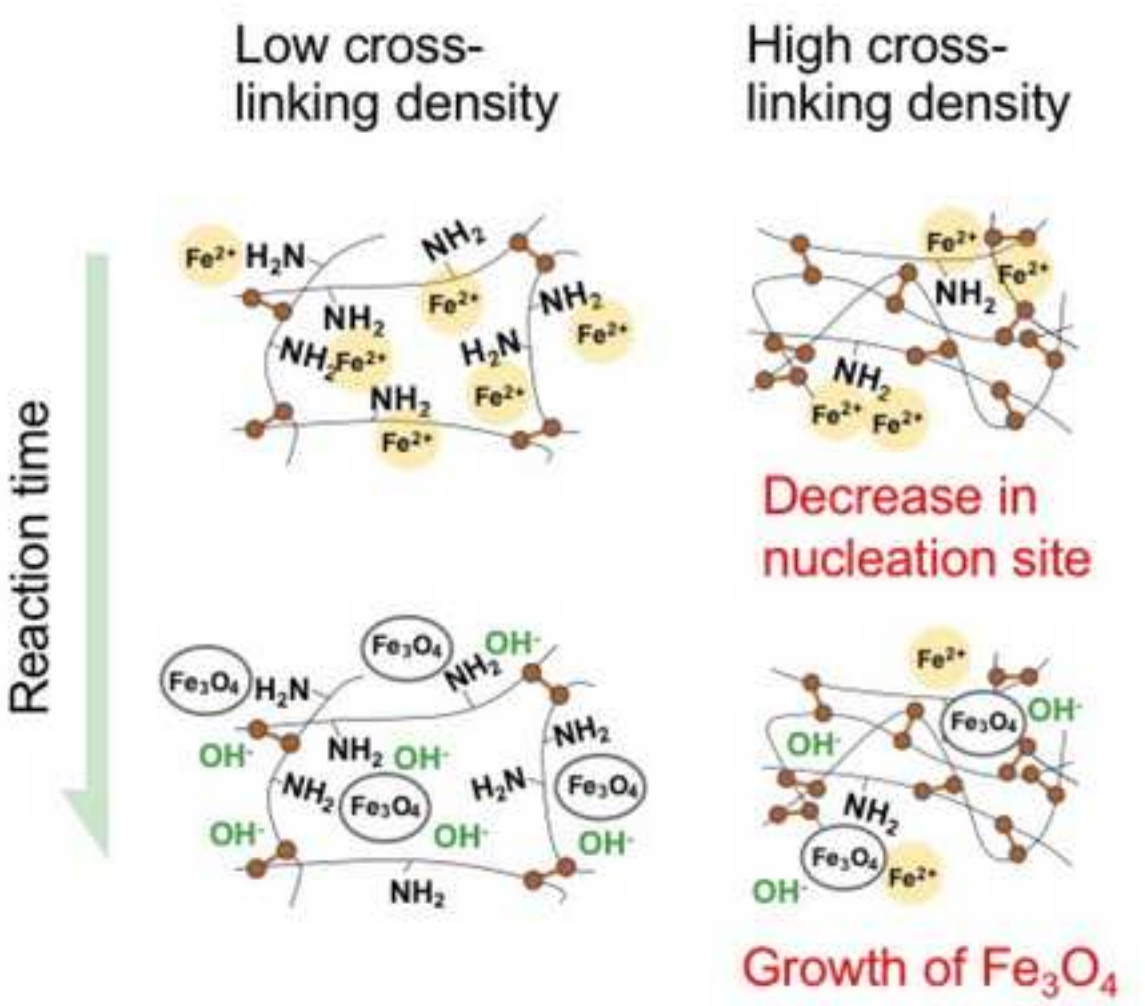

Figure 8